OPEN ACCESS

Original research

ZFYVE19 deficiency: a ciliopathy involving failure of cell division, with cell death

Jing Yang [1,2,3] Ya-Nan Zhang,[1,2] Ren-Xue Wang,[4] Chen-Zhi Hao,[2] Yiling Qiu [1,2] Hao Chi,[1] Wei-Sha Luan [1] HongYi Tang,[5] Xiu-Juan Zhang,[6] XuXu Sun,[5] Jonathan A Sheps,[4] Victor Ling [4] Muqing Cao [6] Jian-she Wang[2,7]

► Additional supplemental material is published online only. To view, please visit the journal online (https://doi.org/10.1136/jmg-2023-109779).

[1]Department of Pediatrics, Jinshan Hospital of Fudan University, Shanghai, China
[2]The Center for Liver Diseases, Children's Hospital of Fudan University, Shanghai, China
[3]Department of Pediatric Gastroenterology, Chengdu Women's and Children's Central Hospital, School of Medicine, University of Electronic Science and Technology of China, Chengdu, China
[4]BC Cancer Agency, Vancouver, British Columbia, Canada
[5]Department of Biochemistry and Molecular Cell Biology, Shanghai Jiao Tong University School of Medicine, Shanghai, China
[6]Department of Pathophysiology, Shanghai Jiao Tong University School of Medicine, Shanghai, China
[7]Shanghai Key Laboratory of Birth Defect, Shanghai, China

Correspondence to
PhD. MD. Jian-she Wang; jshwang@shmu.edu.cn
Dr Muqing Cao; muqingcao@sjtu.edu.cn
Victor Ling; vling@bccrc.ca

JY and Y-NZ are joint first authors.

Received 30 November 2023
Accepted 4 April 2024
Published Online First 30 May 2024

To cite: Yang J, Zhang Y-N, Wang R-X, *et al*. *J Med Genet* 2024;**61**:750–758.

ABSTRACT

Background and aims Variants in *ZFYVE19* underlie a disorder characterised by progressive portal fibrosis, portal hypertension and eventual liver decompensation. We aim to create an animal model to elucidate the pathogenic mechanism.

Methods *Zfyve19* knockout (*Zfyve19*$^{-/-}$) mice were generated and exposed to different liver toxins. Their livers were characterised at the tissue, cellular and molecular levels. Findings were compared with those in wild-type mice and in ZFYVE19-deficient patients. *ZFYVE19* knockout and knockdown retinal pigment epithelial-1 cells and mouse embryonic fibroblasts were generated to study cell division and cell death.

Results The *Zfyve19*$^{-/-}$ mice were normal overall, particularly with respect to hepatobiliary features. However, when challenged with α-naphthyl isothiocyanate, *Zfyve19*$^{-/-}$ mice developed changes resembling those in ZFYVE19-deficient patients, including elevated serum liver injury markers, increased numbers of bile duct profiles with abnormal cholangiocyte polarity and biliary fibrosis. Failure of cell division, centriole and cilia abnormalities, and increased cell death were observed in knockdown/knockout cells. Increased cell death and altered mRNA expression of cell death-related signalling pathways was demonstrated in livers from *Zfyve19*$^{-/-}$ mice and patients. Transforming growth factor-β (TGF-β) and Janus kinase-Signal Transducer and Activator of Transcription 3 (JAK-STAT3) signalling pathways were upregulated in vivo, as were chemokines such as C-X-C motif ligands 1, 10 and 12.

Conclusions Our findings demonstrated that ZFYVE19 deficiency is a ciliopathy with novel histological features. Failure of cell division with ciliary abnormalities and cell death activates macrophages and may thus lead to biliary fibrosis via TGF-β pathway in the disease.

WHAT IS ALREADY KNOWN ON THIS TOPIC

⇒ ZFYVE19 deficiency causes a type of progressive familial intrahepatic cholestasis, characterised by specific liver abnormalities. However, the direct mechanistic links between ZFYVE19 loss and liver pathology were not fully understood.

WHAT THIS STUDY ADDS

⇒ Our research demonstrates that ZFYVE19 deficiency leads to significant liver pathology only on challenge with a hepatotoxic agent, which suggests a facultative ciliopathy. We also discovered novel histological features indicative of a failure in cell division and increased cell death, potentially contributing to the observed biliary fibrosis in patients.

HOW THIS STUDY MIGHT AFFECT RESEARCH, PRACTICE OR POLICY

⇒ These insights could influence future research by identifying new therapeutic targets within the transforming growth factor-β signalling pathway and macrophage activation. Clinically, our study suggests new diagnostic markers for liver pathology associated with ZFYVE19 mutations and highlights the importance of environmental factors in the manifestation of genetic diseases.

INTRODUCTION

Biallelic complete loss-of-function variants in *ZFYVE19* (MIM *619635) are associated with a type of progressive familial intrahepatic cholestasis (MIM #619849) characterised by conjugated hyperbilirubinemia, hypercholanemia, high serum activity of γ-glutamyl transpeptidase (GGT) and portal tract abnormalities that include increased numbers of bile ducts, cholangiocyte disarray with abnormal bile duct contours, portal venule hypoplasia and fibrous expansion, as encountered in congenital hepatic fibrosis.[1] These abnormalities constitute the ductal plate malformation (DPM). Over time, portal inflammation, portal fibrosis and bile duct loss develop.[1 2] The presentation may be associated with neonatal cholestasis[3] or abnormal biomarker values that reflect hepatobiliary injury in older children or adults.[4]

ZFYVE19 (also known as ANCHR) and CHMP4C recruit VPS4 into the mid-body ring to regulate cytokinesis.[5] Patient-derived cells that harbour biallelic complete loss-of-function variants in *ZFYVE19* show ciliary and centriolar abnormalities.[1 3] How the absence of a protein regulating cell division contributes to portal tract fibrosis is not understood. The developmental consequences of ZFYVE19 deficiency and their mechanisms need further study.

In the work described here, we generated a *Zfyve19*$^{-/-}$ mouse model to investigate in mechanistic detail the role of loss of Zfyve19. Though the fetal development of intrahepatic bile ducts (IHBD)

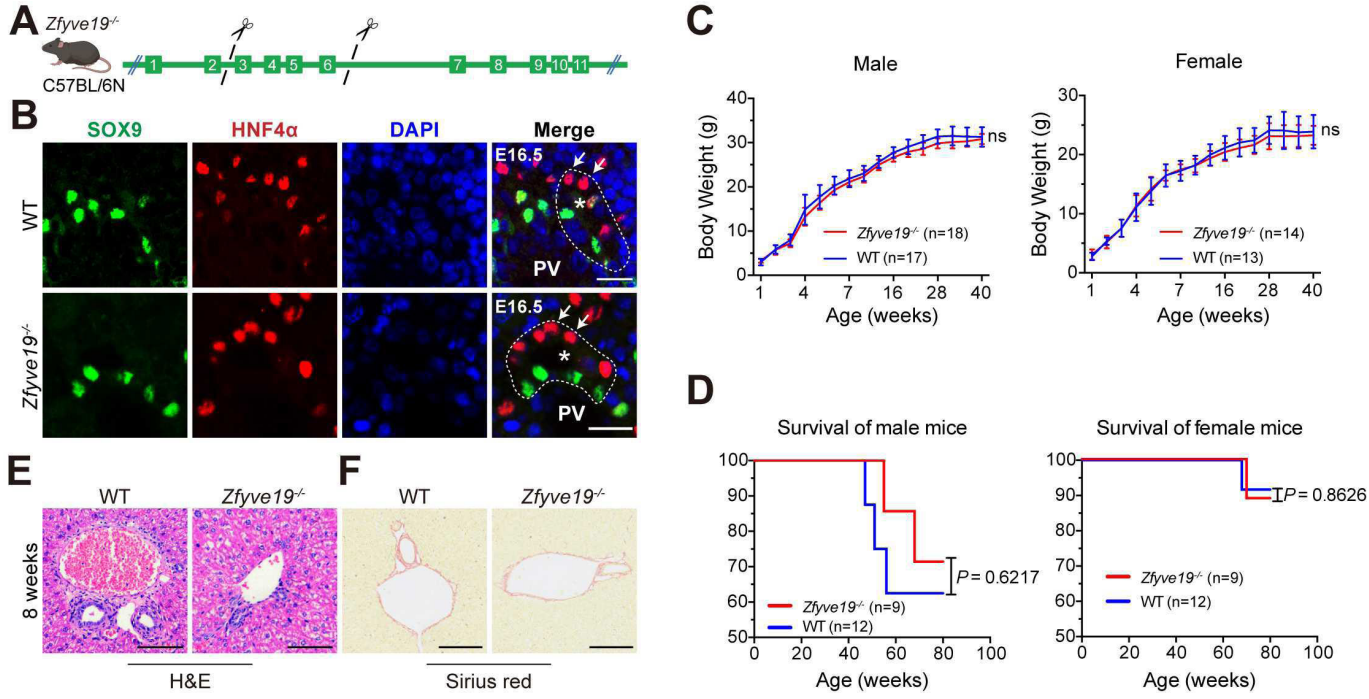

Figure 1 *Zfyve19*$^{-/-}$ mice show no defects in embryonic bile duct development and early postnatal phenotype. (A) *Zfyve19* locus targeting scheme. (B) Immunofluorescence costaining of SOX9 and HNF4α in both *Zfyve19*$^{-/-}$ and wild-type (WT) mouse livers at embryonic day 16.5 (E16.5). PV, portal vein. *Bile-duct lumen; dashed line, nascent tubules. Bars: 20 µm. (C) Body weight (g) measurements over 40 weeks in both female and male *Zfyve19*$^{-/-}$ mice compared with WT littermates. Data are shown as mean±SD. (D) Kaplan-Meier survival curves over 80 weeks in *Zfyve19*$^{-/-}$ mice compared with WT littermates of both sexes. (E,F) Mouse liver, age 8 weeks, stained with H&E and Sirius Red. Bars: 100 µm. ns, not significant.

is normal, the knockout mice show histopathologic features characteristic of ZFYVE19-deficient patients on α-naphthyl isothiocyanate (ANIT) challenge after birth. The absence of *ZFYVE19*/*Zfyve19* expression causes failure of cell division, with ciliary and centriolar abnormalities, and to cell death, thus initiating the process of biliary fibrosis. Our findings demonstrate that ZFYVE19 deficiency may be a ciliopathy with hepatobiliary manifestations that begin after birth.

MATERIALS AND METHODS

Animal care

Mice used in this study were housed at an ambient temperature of approximately 22°C and subjected to 12-hour light-dark cycles. No more than five mice were housed in one cage, and free access to food and water was given. Mice were sacrificed by terminal anaesthesia with isoflurane, followed by cervical dislocation. All experiments were performed using age-matched littermate mice.

Generation of *Zfyve19* knockout (*Zfyve19*−/−) mice

Since to date all patients with ZFYVE19 deficiency investigated harbour biallelic null mutations in *ZFYVE19*, we decided to produce a knockout mouse with complete loss of Zfyve19 function (*Zfyve19*$^{-/-}$ mouse), using CRISPR/Cas9 technology on a C57BL/6N background (figure 1A). Small guide RNAs (sgRNAs) were 5′-CCTTGTGGCCTTGTGCGCCCTGG-3′ and 5′-GGAGCGGGCAACTGCACGGTAGG-3′. Deletion of exon 3–6 of the *Zfyve19* (GenBank ID: NM 028054.3; Ensembl: ENSMUSG00000068580) was predicted, leading to mRNA nonsense-mediated decay. Successful depletion of *Zfyve19* was confirmed at the DNA (online supplemental figure 1A), mRNA (online supplemental figure 1B,C) and protein levels (online supplemental figure 2A,B).

ANIT treatment in mice

20 male mice (6–8 weeks of age, 18–22 g) were used, 10 *Zfyve19*$^{-/-}$ (groups 1 and 2, 5 mice each) and 10 wild type (WT) (groups 3 and 4, 5 mice each). On days 0, 7 and 14, mice in groups 1 and 3 were given the liver toxin ANIT (Sigma-Aldrich), 60 mg/kg, in olive oil vehicle via intragastric sonde; mice in groups 2 and 4 were similarly given vehicle at the same dose. Between 36 and 48 hours after the final dose, mice were fasted for 4 hours and euthanised; samples were collected (figure 2A).

Human samples

Tissues from three ZFYVE19-deficient patients (P14, P29 and P30) and three patients harbouring biallelic *ABCB4* variants—ABCB4 deficiency, such as ZFYVE19 deficiency, presents as high-GGT cholestasis with cholangiopathy—all obtained from explanted livers, were studied, with normal donors as controls. All subjects or parents provided written informed consent.

Generation of *ZFYVE19* knockout and knockdown retinal pigment epithelial-1 (RPE-1) cells

Human RPE-1 cells ('hTERT RPE-1', CRL-4000; ATCC, Manassas, Virginia, USA) were cultured in Dulbecco's Modified Eagle Medium/Nutrient Mixture F-12 (DMEM/F12) (Biological Industries) with 5% Fetal Bovine Serum (FBS) (Gibco) under 5% CO_2. sgRNAs (5′-CACCGCGACCCTGGACGCAACCCCG-3′ and 5′- AAACCGGGGTTGCGTCCAGGGTCGC-3′) targeting *ZFYVE19* were inserted into a modified lentiCRISPRv2 vector (AddGene #98293). Lentivirus were produced by cotransfection of lentiCRISPRv2-sgRNA plasmids pCMV-VSVG (AddGene #8454) and psPAX2 (AddGene #12260). Media containing lentivirus were added to the RPE-1 cells' culture medium when cells were grown to 50% confluence. Blasticidin (Meilunbio)

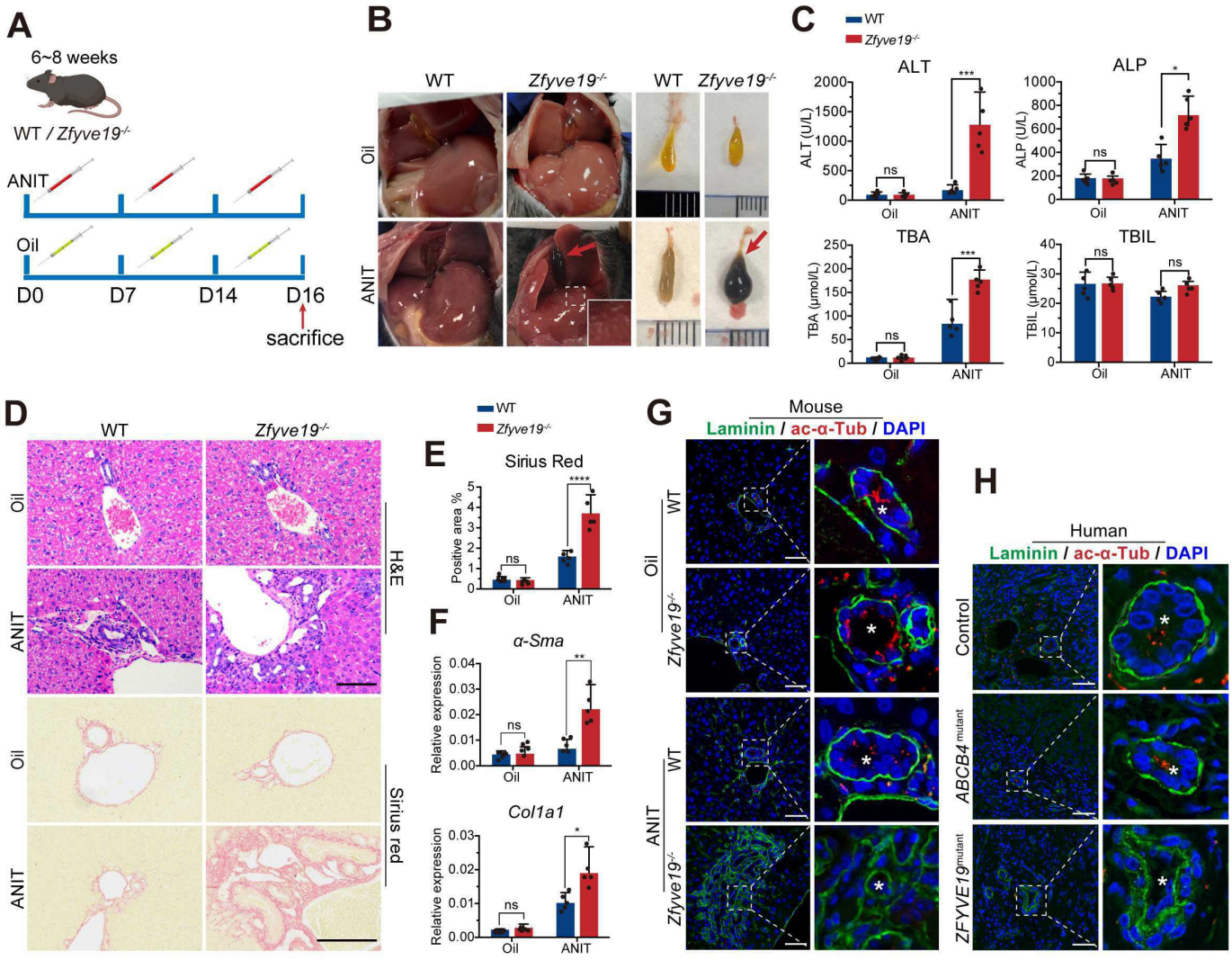

Figure 2 Biliary fibrosis and disordered cholangiocyte polarity in liver of *Zfyve19*$^{-/-}$ mice after α-naphthyl isothiocyanate (ANIT) challenge. (A) Schematic experimental outline. Mice per treatment group, n=5–6. (B) Appearance of representative livers and gallbladders. The inset shows a region with severe liver lesions. The enlarged gallbladder is marked by a red arrow. (C) Serum alanine aminotransferase (ALT), alkaline phosphatase (ALP), total bile acid (TBA), and total bilirubin (TBIL) levels. (D) Representative H&E and Sirius Red-stained liver sections. Bars: 100 µm. (E) Plot of per cent area of Sirius Red staining in livers from *Zfyve19*$^{-/-}$ and wild-type (WT) mice after ANIT treatment. (F) RT-qPCR of α-Sma and Col1a1 in livers from *Zfyve19*$^{-/-}$ and WT mice (n=5–6). (G) Immunofluorescence costaining of laminin and acetylated α-tubulin (ac-α-Tub) in mouse livers. Bars: 50 µm. *Bile duct lumen. (H) Immunofluorescence costaining of laminin and ac-α-Tub in liver from patients with *ZFYVE19* variants (*ZFYVE19*^{mutant}) or *ABCB4* variants (*ABCB4*^{mutant}) and from healthy controls. Bars: 50 µm. *bile duct lumen. Data are shown as mean±SD. ns, not significant, *p<0.05, **p<0.01, ***p<0.001 or ****p<0.0001.

was added to the culture medium 48 hours after infection, to a final concentration of 30 µg/mL. After 2 weeks of blasticidin selection, colonies formed by single cells were picked out and assessed for *ZFYVE19* knockout by western blot.

To knock down the endogenous expression of *ZFYVE19*, siRNAs specific for *ZFYVE19* were designed (siRNA1: 5′-GGAU GAGGCAAGUGGCUUUTT-3′ and 5′-AAAGCCACUUGC CUCAUCCTT-3′; siRNA2: 5′-UCACCACCUCAGAACUAUATT-3′ and 5′-UAUAGUUCUGAGGUGGUGACC-3′). The non-targeting siRNAs (5′-GCGACGAUCUGCCUAAGAUdTdT-3′ and 5′-AUC UUAGGCAGAUCGUCGCdTdT-3′) were used as negative controls. siRNA oligonucleotides were complexed with Lipofectamine RNAiMAX transfection reagent (Invitrogen) in Opti-MEM medium (Invitrogen) and were added to the medium when the cells were grown to ~50% confluence in penicillin-free and streptomycin-free DMEM/F12 complete medium (Gibco). The final siRNA concentration was 20 nM. After 72 hours, cells were fixed for immunofluorescence (IF) microscopy or harvested to assess *ZFYVE19* knockdown efficiency by western blot (figure 3A).

Mouse embryonic fibroblasts (MEFs)

MEFs were cultured in DMEM (Sigma) with 10% FBS (Gibco). WT MEFs and *Zfyve19*$^{-/-}$ MEFs were generated from WT and *Zfyve19*$^{-/-}$ mice, respectively. Mice were mated at 8–12 weeks of age and embryos were allowed to develop for 13.5–15.5 days (E13.5–E15.5). Embryonic thoracic wall tissues were used to generate an MEF cell suspension by incubation in 0.25% trypsin (Ethylenediaminetetraacetic acid (EDTA) free) at 37°C for 30 min. The MEF cell suspension was centrifuged at 1000 rpm for 5 min, washed in phosphate-buffered saline once and resuspended in complete culture medium.

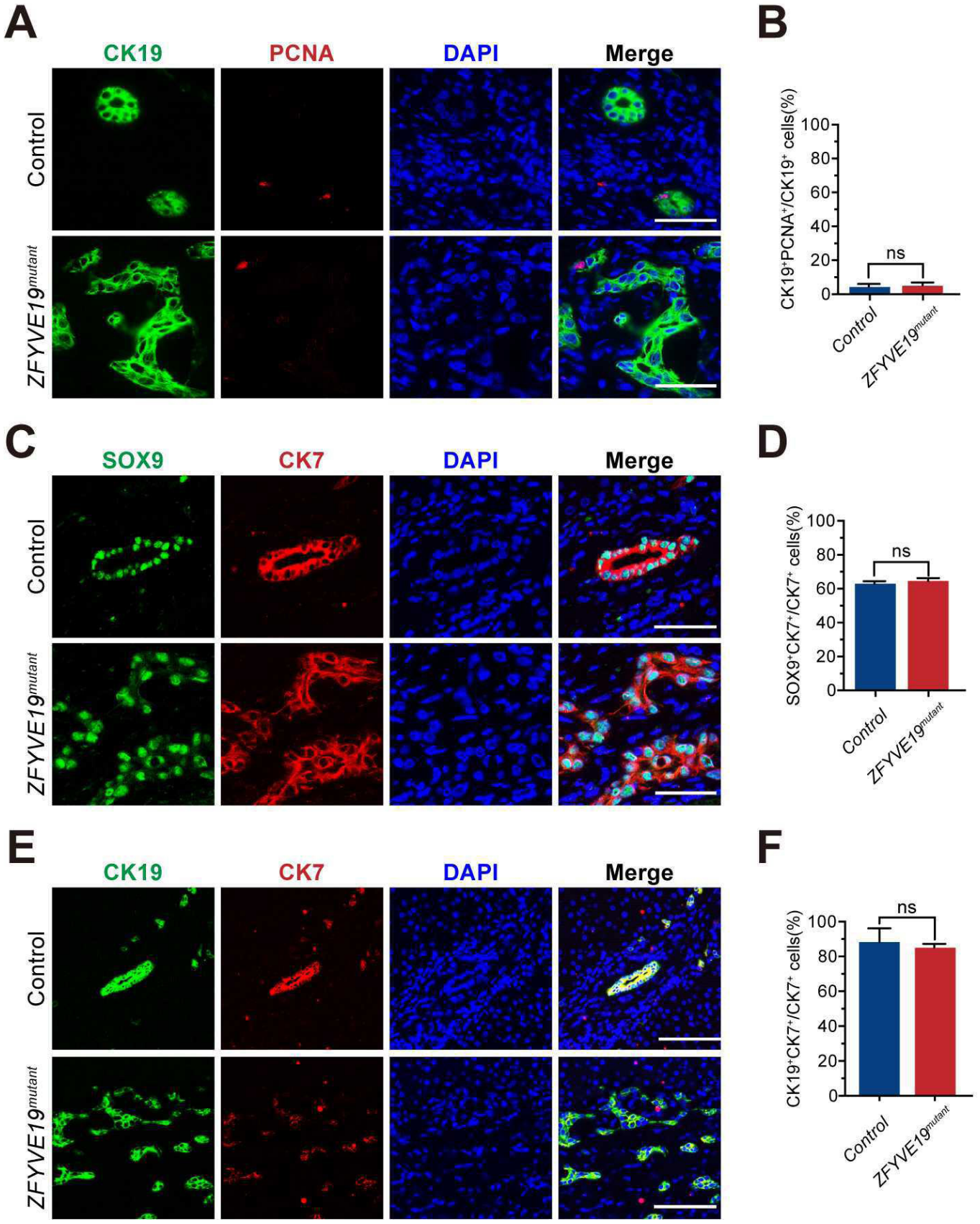

Figure 3 Effect of *ZFYVE19* defects on proliferation, maturity and differentiation of cholangiocytes in *ZFYVE19*-variant patients. Immunofluorescence photomicrographs of liver, PCNA and CK19 ((A) scale bar: 100 µm); SOX9 and CK7 ((C) scale bar: 50 µm); and CK19 and CK7 ((E) scale bar: 50 µm), ZFYVE19-deficient patient and normal donor (control). DAPI, 4′,6-diamidino-2-phenylindole. Histograms, $CK19^+PCNA^+$ cells as a percentage of total $CK19^+$ cells (B); $SOX9^+CK7^+$ cells as a percentage of total $CK7^+$ cells (D); and $CK19^+CK7^+$ cells as a percentage of total $CK7^+$ cells (F). Data are shown as mean±SD. ns, not significant.

DNA content assay

For DNA content assay by flow cytometry, cells were suspended in a 1:9 mixture of RNase A and propidium iodide (PI) reagent (Keygentec). The cells were immediately sorted by flow cytometry (Beckman). Flow cytometry data were analysed using ModFit LT V.5.0.

Measuring cell death by flow cytometry and transferase-mediated deoxyuridine triphosphate nick-end labelling (TUNEL) assay

Fluorescence-activated cell sorting with flow cytometry analysis of PI-stained cells was used to measure cell death as described.[6]

Fluorescent terminal deoxynucleotidyl TUNEL assayed dead cells in paraffin-embedded sections (4 µm) of liver tissues. Dead cells in portal areas were quantified by counting $TUNEL^+$ cells per viewfield in at least 10 random microscope fields (15×) of portal tract areas, using a Panoramic MIDI histoscanner (3DHistech).

Serum biochemistry analysis, quantitative real-time PCR, RNA-Seq, western blotting analysis, histopathological staining and IF staining

See online supplemental material.

Statistical analysis

Statistical analysis used GraphPad Prism V.6.0 software (GraphPad). All data are presented as means±SD. Continuous data were tested for normality and analysed by unpaired Student's t-tests, Mann-Whitney U testing or one-way analysis of variance (ANOVA), as appropriate. Differences within and between groups were evaluated using two-way ANOVA. Survival was assayed by Kaplan-Meier and log-rank analyses. Statistical significance is displayed as ns (not significant), *p<0.05, **p<0.01, ***p<0.001 or ****p<0.0001, unless specified otherwise.

RESULTS

Zfyve19–/– mice and WT littermates show no obvious differences in bile duct development and postnatal growth

Zfyve19$^{-/-}$ mice were generated by CRISPR/Cas9 deletion of exons 3–6 of *Zfyve19* (figure 1A). The development of IHBD is characterised by asymmetric expression of the expanded bile duct and hepatoblast cell markers, respectively, SOX9 on the internal side and HNF4α on the external side of the ductal plate (~E16 P2).[6–8] IF staining of SOX9 and HNF4α in E16.5 *Zfyve19*$^{-/-}$ mice showed normal bile duct lumina. Ductal plate cells exhibited typical asymmetry in nascent tubules, with SOX9-expressing cells near the portal vein and HNF4α-expressing cells contralaterally (figure 1B). These developmental features did not differ from those of IHBD in WT littermates.

To assess growth, mice were weighed once a week during postnatal weeks 1–8 after birth and once every 4 weeks thereafter until age 40 weeks. Weights of *Zfyve19*$^{-/-}$ mice of either gender did not differ from those of WT littermates (figure 1C). Survival rates of *Zfyve19*$^{-/-}$ mice of either gender (up to 80 weeks) also did not differ from those of WT littermates (figure 1D). Hepatobiliary development as assessed by light microscopy did not differ at age 8 weeks between male *Zfyve19*$^{-/-}$ mice and WT littermates; cholestasis, bile duct proliferation, necrotic hepatocytes and hepatic fibrosis were not seen (figure 1E,F). Loss of *Zfyve19* expression in mouse thus led to no identified systemic or liver-restricted abnormalities.

Features of liver injury, with biliary fibrosis and cholangiocyte disarray resembling lesions in ZFYVE19-deficient patients, are prominent after ANIT treatment in *Zfyve19*–/– mice

Zfyve19$^{-/-}$ mice were exposed to different liver toxins. With ANIT administration (figure 2A, see Material and methods for details), *Zfyve19*$^{-/-}$ mice trended towards greater loss of body weight and greater liver: body weight ratio at endpoint than those in WT littermates, although without differences that reached statistical significance (online supplemental figure 3A, B). However, livers of *Zfyve19*$^{-/-}$ mice were firmer than those of WT littermates, with more visible liver lesions (nodularity distributed throughout the liver), larger gallbladders and darker bile (figure 2B). The levels of serum ALT and ALP activity and total bile acid (TBA) concentrations, but not total bilirubin (TBIL) concentrations, were significantly higher in *Zfyve19*$^{-/-}$ mice than in WT littermates after ANIT challenge, while no differences were observed between *Zfyve19*$^{-/-}$ and WT mice with oil vehicle control (figure 2C).

Though histopathologic study showed no hepatobiliary anomalies in *Zfyve19*$^{-/-}$ mice and no differences from WT mice treated with vehicle controls, after ANIT treatment, more numerous necrotic hepatocytes, denser inflammatory infiltration, increased numbers of bile duct profiles on H&E staining (figure 2D), significantly more severe fibrosis on Sirius Red staining (figure 2D,E) and higher (approximately fourfold) mRNA expression of profibrosis genes *α-Sma* and *Col1a1* (figure 2F) were seen in *Zfyve19*$^{-/-}$ mice than in WT mice. The expression of *α-SMA* and *COL1A1* mRNA was consistently higher in livers of ZFYVE19-deficient patients than in normal controls (online supplemental figure 4), consonant with findings in mice.

Patients with biallelic complete loss-of-function *ZFYVE19* variants exhibit DPM.[1] DPM is generally associated with cholangiocyte-polarity disorders.[7 8] IF costaining for laminin, a basally expressed antigen, and acetylated (ac)-α-tubulin (ac-α-Tub), an apically expressed antigen, accordingly was used to assess cholangiocyte apical–basal polarity. In vehicle-treated *Zfyve19*$^{-/-}$ and WT mice and in ANIT-treated WT mice, laminin adjoined the basement membrane of bile ducts and ac-α-Tub adjoined bile duct lumina (figure 2G). However, ANIT-treated *Zfyve19*$^{-/-}$ mice showed abnormal apical–basal cholangiocyte polarity: laminin localisation was disordered and ac-α-Tub signalling was obviously reduced or even absent at bile duct lumina (figure 2G).

To learn if the polarity disruption seen in ANIT-treated *Zfyve19*$^{-/-}$ mice was present in patients with ZFYVE19 deficiency, IF staining for laminin and ac-α-Tub was conducted in the livers of three such patients and of three patients with *ABCB4* disease, a disorder clinically characterised by cholestasis with high serum GGT and abnormally numerous bile duct profiles, and in the livers of healthy controls. We found that the healthy controls without biliary fibrosis and the patients with *ABCB4* variants, whose livers showed biliary fibrosis, had normal laminin and ac-α-Tub distributions in bile ducts (figure 2H). In contrast, laminin signalling in patients with ZFYVE19 deficiency lay principally at non-basal sites within cholangiocytes, while ac-α-Tub at bile duct lumina was markedly less strongly expressed than normal or even absent entirely (figure 2H). These findings demonstrate that the polarity disruption seen in ANIT-treated *Zfyve19*$^{-/-}$ mice is also present in patients with

ZFYVE19 deficiency, suggesting that the *Zfyve19*$^{-/-}$ mouse may, as a model, track human disease.

IF staining for the mature cholangiocyte marker CK19 showed increased number of bile duct profiles in ZFYVE19-deficient patients (figure 3). IF staining for SOX9 (a marker of regeneration of hepatocytes and cholangiocytes) and CK7 (a mature and immature cholangiocyte marker) showed increased to similar degrees of CK19 expression (figure 3C–F). However, IF costaining did not reveal increased marking for PCNA, a proliferation-associated antigen (figure 3A,B). The expression of *Pcna* mRNA in ANIT-treated *Zfyve19*$^{-/-}$ mice did not differ from that in WT controls (online supplemental figure 5).

ZFYVE19 depletion/deletion causes failure of cell division and cell death

ZFYVE19 acts as a key regulator of cytokinesis.[5] To examine the effects of ZFYVE19 deficiency on cell division, *ZFYVE19*-targeting siRNA was used to deplete ZFYVE19 in RPE-1 cells (online supplemental figure 6A). *ZFYVE19* knockdown induced a significant increase in proportions of cells with DNA content>2N and <4N (online supplemental figure 6B,C). IF staining showed that the proportion of cells with three or four centrioles (CP110^{+}) was significantly increased, by at least fourfold, in ZFYVE19 knockdown cells (online supplemental figure 6D,E). Similar results were observed in *ZFYVE19* knockout RPE-1 cells (online supplemental figure 6A–E) and *Zfyve19*$^{-/-}$ MEFs (online supplemental figure 7A–C).

The failure of cell division can cause overduplication of centrioles. The duplicated centrioles express CEP170, a marker of mature centrioles. Costaining for CP110 and CEP170 was performed (online supplemental figure 8A). The proportion of cells with >2 centrioles of which >1 marked for CEP170 was significantly greater among *ZFYVE19* knockout RPE-1 cells than among controls (online supplemental figure 8B). This indicates that centrioles are overduplicated in *ZFYVE19* knockout cells, in agreement with greater numbers of double cilia in *ZFYVE19* knockout RPE-1 cells than in controls (online supplemental figure 8C,D) and in *Zfyve19*$^{-/-}$ MEFs than in WT MEFs (online supplemental figure 8E,F).

Both defects of centrosome splitting and failure of cell division cause cell death.[9–11] Since biliary fibrosis in livers with ZFYVE19 deficiency might reflect an inflammatory response induced by cell death, PI uptake in *ZFYVE19* knockdown RPE-1 cells was measured by flow cytometry. Depletion of ZFYVE19 in RPE-1 cells led to more cell death (figure 4F,G). To determine the levels of cell death in vivo, TUNEL assays were performed in mouse and human liver sections. A number of dead cells in the portal areas of the liver in ANIT-treated *Zfyve19*$^{-/-}$ mice were significantly higher (greater than threefold) than in ANIT-treated WT mice. No difference between vehicle-treated *Zfyve19*$^{-/-}$ and WT mice was observed (figure 4H,I). Consistent with this, TUNEL assays found substantially more dead cells (>20-fold) in the portal areas of liver from ZFYVE19-deficient patients than in those from healthy controls (figure 4J,K).

Moreover, gene set variation analysis (GSVA) on mRNA-seq in livers of ZFYVE19-deficient patients and livers from ANIT-treated *Zfyve19*$^{-/-}$ mice showed alterations in cell division-related and cell death-related signalling pathways (G2/M-checkpoint, DNA-repair and mitotic-spindle signalling pathways) (online supplemental figure 9 and figure 5A).

Transforming growth factor-β (TGF-β) signalling pathway and macrophage chemokine synthesis are up-regulated in *ZFYVE19*-variant livers

To explore the pathways and genes involved in fibrosis, we applied GSVA to mRNA-seq data from the livers of ZFYVE19-deficient patients and of *Zfyve19*$^{-/-}$ mice. GSVA showed significant upregulation of the TGF-β signalling pathway in ZFYVE19-deficient patients (online supplemental figure 9). In *Zfyve19*$^{-/-}$ mice gavaged with ANIT the TGF-β and JAK-STAT3 signalling pathways were up-regulated in comparison with control mice (figure 5A); these pathways are important in regulating liver fibrosis and macrophage activation.[12 13] RT-qPCR of mouse liver tissue confirmed these results. *Tgfβ1* mRNA, but not *Tgfβ2* mRNA, was more abundant in ANIT-induced *Zfyve19*$^{-/-}$ mice than in ANIT-exposed WT mice (figure 5B). The expression of *Itgb6/8* (activators of latent TGFβ1) and of *Ctgf,* downstream from *Tgfβ* in a desmoplastic cascade, was also increased at the mRNA level in ANIT-exposed *Zfyve19*$^{-/-}$ mice (figure 5B). *TGFβ1*, *CTGF* and *ITGB6/8* mRNA levels in the livers of ZFYVE19-deficient patients were consistently increased as well (figure 5C). The levels of SMAD2 and its activated form, p-SMAD2, which are TGFβ signalling pathway downstream regulators, were increased in patient liver (online supplemental figure 10A).

In contrast, expression in mouse liver of other genes related to hepatic fibrosis, *for* example, *Yap* (Hippo signalling pathway), *β-Catenin* (Wnt signalling pathway), *Jnk*, *Rock2* (planar cell polarity pathway) and *PDGFα*, did not vary from controls (online supplemental figure 11). We therefore conclude that the TGF-β and JAK-STAT3 signalling pathways may be principally involved in biliary fibrosis in ZFYVE19 deficiency.

Consistent with mRNA sequencing data, RT-qPCR results showed that after ANIT treatment expression of macrophage chemotactic factors (*Cxcl1*, *Cxcl10*, *Cxcl12* and *Ccl2*) and of the proinflammatory cytokine *Il-1β* increased in liver of *Zfyve19*$^{-/-}$ mice (figure 5D), while no significant difference in *Il-1β* expression was observed in ZFYVE19-deficient patients (online supplemental figure 10B). Although the expression of inflammatory factor *Tnf-α* in *Zfyve19*$^{-/-}$ mice also increased, no statistical significance was attained. The expression of another inflammatory factor, *Il-6*, was similar among all four groups (figure 5D).

DISCUSSION

A recently identified association between biallelic loss-of-function *ZFYVE19* variants and a type of high-GGT portal fibrosis histopathologically characterised by DPM has been confirmed.[3 4] However, no animal model has existed. The work presented here—generation of a *Zfyve19*$^{-/-}$ mouse in which, on ANIT administration, the human ZFYVE19-deficiency phenotype is recapitulated—provides mechanistic insight into the causal relationship between ZFYVE19 deficiency and the observed disease.

Zfyve19$^{-/-}$ mice without challenge did not manifest the liver phenotype of ZFYVE19-deficient patients. Traditionally, when phenotypes in knockout mice do not recapitulate phenotypes in patients with lesions in orthologous genes, toxins are often used to induce phenotype development. For example, in *Abcb11* knockout mice, cholic acid feeding induces ABCB11-deficiency-like phenotypes.[14] *Zfyve19*$^{-/-}$ mice on cholic acid feeding did not have the liver phenotype of ZFYVE19-deficient patients (data not shown). ANIT is a biliary toxin used to study acute (high and single dose) and chronic (low dose, ≥4 weeks) bile duct injury in mice.[15] With three times weekly low-dose

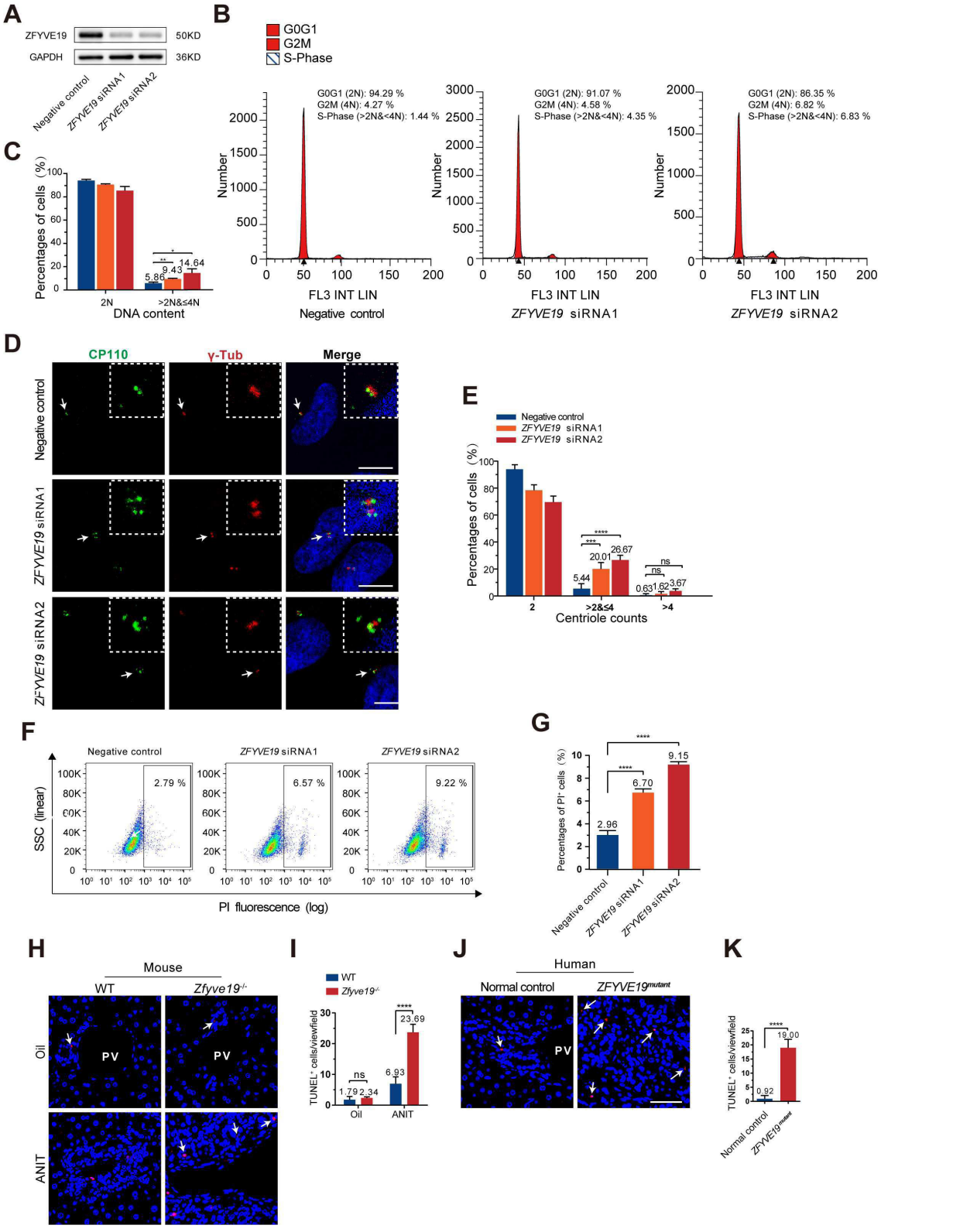

Figure 4 Failure of cell division and cell death after ZFYVE19 depletion/suppression. (A) Western blot of ZFYVE19 in retinal pigment epithelial-1 (RPE-1) cells. (B) Representative cell cycle distributions in *ZFYVE19* knockdown RPE-1 cells, measured by DNA content; flow cytometry analysis. (C) Histogram, cell cycle distribution in *ZFYVE19* knockdown RPE-1 cells in (B). (D) Immunofluorescence (IF) costaining for CP110 and γ-tubulin (γ-Tub) in *ZFYVE19* knockdown RPE-1 cells. Bars: 10 µm. (E) Percentages of *ZFYVE19* knockdown RPE-1 cells with different numbers of centrioles (CP110+). (F) Cell death in *ZFYVE19* knockdown RPE-1 cells measured by flow cytometry. (G) Percentages of propidium iodide-marked cells in *ZFYVE19* knockdown RPE-1 cells. (H) IF, $TUNEL^+$ cells (arrows) in portal tracts in the livers of WT and $Zfyve19^{-/-}$ mice after oil or 1-naphthyl isothiocyanate treatment. (I) Number of $TUNEL^+$ cells per viewfield (15×) from mouse tissues (n=3–5). (J) IF, periportal $TUNEL^+$ cells (arrows) in liver from *ZFYVE19*-variant patients (n=3). (K) Number of $TUNEL^+$ cells per viewfield (15×) in liver sections from *ZFYVE19*-variant patients. Bars: 50 µm. Data are shown as mean±SD. ns, not significant, *p<0.05, **p<0.01, ***p<0.001 or ****p<0.0001.

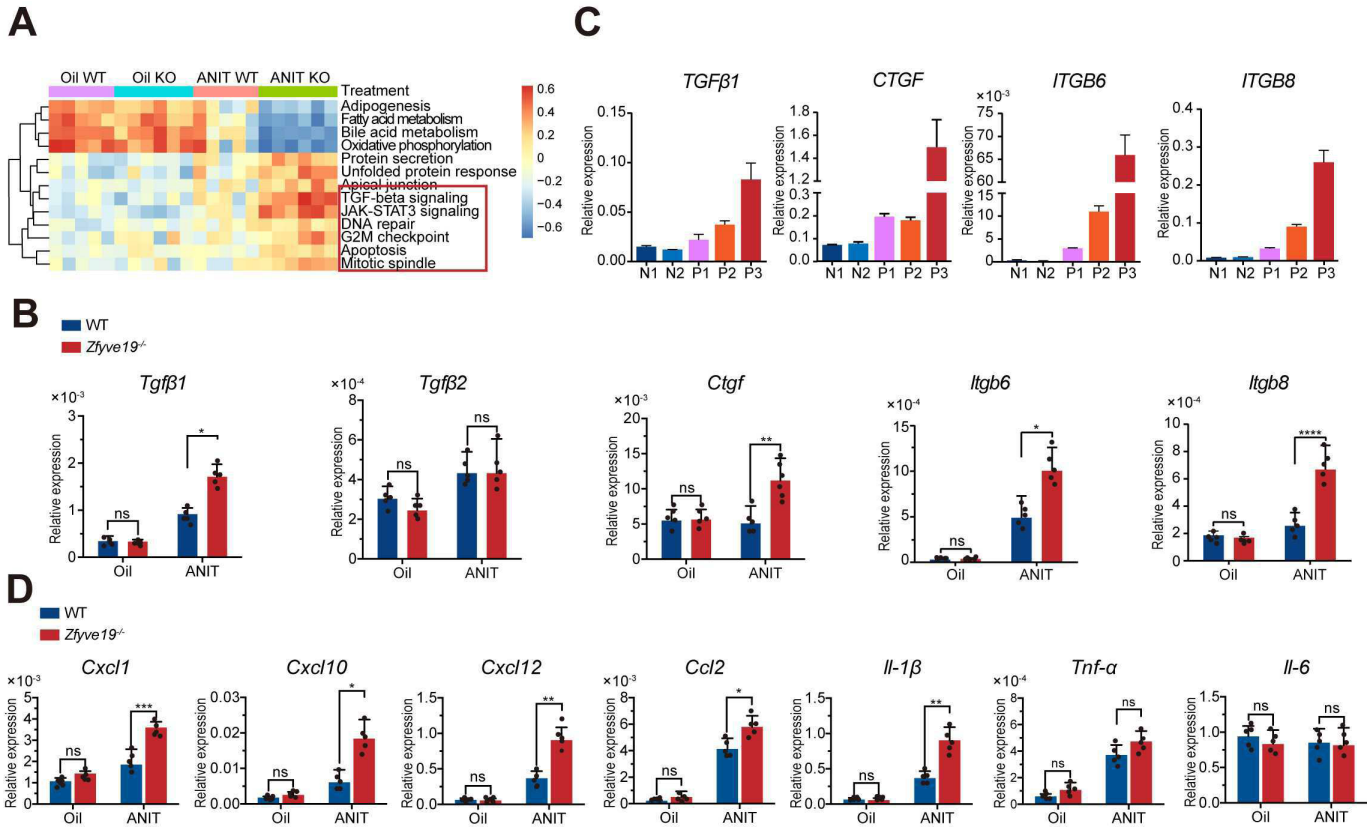

Figure 5 Changes in signal pathways regulating hepatic fibrosis and macrophage activity in ZFYVE19-deficient and Zfyve19-deficient liver. (A) Gene set variation analysis of signal pathways in mouse liver from 4 groups (n=5–6). (B,C) Expression of genes in the transforming growth factor-β (TGF-β) pathway tested using RT-qPCR in mouse liver (n=5–6) and human liver. (D) Relative mRNA expression levels of macrophage chemokine genes, including *Cxcl1*, *Cxcl10*, *Cxcl12* and *Ccl2* and proinflammatory cytokines, including *Il-1β*, *Tnf-α* and *Il-6* by RT-qPCR in mouse liver (n=5–6). KO, knockout (*Zfyve19*$^{-/-}$). WT, wild-type. Data are shown as mean±SD. ns, not significant, *p<0.05, **p<0.01, ***p<0.001 or ****p<0.0001.

intragastric administration of ANIT, *Zfyve19*$^{-/-}$ mice developed elevated serum ALT and ALP activities and TBA concentrations (figure 2C) with IHBD abnormalities (figure 2D), portal tract inflammation (figure 2D) and portal tract fibrosis (figure 2E,F), findings resembling those in *ZFYVE19*-disease patients[1].

Anomalies of cholangiocyte polarity, often associated with DPM, were then identified in ANIT-treated *Zfyve19*$^{-/-}$ mice. These anomalies were further demonstrated in ZFYVE19-deficient patients, but not in explanted livers from patients with *ABCB4* variants. These results indicate that disordered cholangiocyte polarity was associated with *ZFYVE19*/*Zfyve19* defects rather than simply with inflammatory cholangiopathy.

ZFYVE19 (ANCHR) was originally identified as a key component of cytokinesis during cell division, associated with Aurora-B-dependent abscission checkpoint control.[5] Failure of cell division presumably equips cells with supernumerary 'mother centrioles' that become basal bodies for supernumerary cilia.[16] Consistent with identification of abnormal centrioles in ZFYVE19-deficient patient-derived cells,[1] ZFYVE19 depletion induced an increase in the number of cells with DNA content>2N, cells with >2 centrioles and cells with >1 mature centriole, suggesting failure of cell division.[17] Both defects of the centrosome and failure of cell division have been related to cell death.[10 18 19] This study demonstrates increased cell death in ZFYVE19-deficient RPE-1 cells, in portal areas of ANIT-treated *Zfyve19*$^{-/-}$ mice and in ZFYVE19-deficient patients. The effects of ZFYVE19 deficiency on cell division and cell death are also supported by RNA-seq data in ZFYVE19-deficient patients and ANIT-treated *Zfyve19*$^{-/-}$ mice that demonstrate upregulation of cell division-related signalling pathways, such as those for the G2/M checkpoint, DNA repair, and mitotic spindle formation.

Increased cell death was demonstrated by ZFYVE19 depletion/deletion in vitro and in vivo (see Results). Various cytokines and chemokines released from dead cells may participate in activation of intrahepatic macrophages, promoting fibrogenesis.[20 21] RNA-seq data in ZFYVE19-deficient patients and ANIT-treated *Zfyve19*$^{-/-}$ mice suggest upregulation of TGF-β and JAK-STAT3 pathways, which are related to fibrosis and to macrophage activation.[22–24] Elevation of *TGF-β1*, *CTGF* and *ITGB6/8* mRNA synthesis, and of SMAD2 and p-SMAD2 expression, in ZFYVE19-deficient patients and ANIT-treated *Zfyve19*$^{-/-}$mice confirms activation of the TGF-β pathway. Moreover, we found that mRNA expression of macrophage chemokines *Cxcl1*, *Cxcl10* and *Cxcl12*, which might participate in the activation of macrophages, increased in *Zfyve19*$^{-/-}$ mouse liver, similar to changes seen in the *Pkhd1* $^{del4/del4}$ mouse (a mouse model of congenital hepatic fibrosis).[21]

CONCLUSION

Zfyve19$^{-/-}$ mice when unchallenged showed no obvious abnormalities but on ANIT administration recapitulated postnatal aspects of ZFYVE19 deficiency, prompting the

hypothesis that ZFYVE19 deficiency may be a ciliopathy manifest on exposure to physiologic 'toxins', in particular the components of postnatal bile. New histological features of ZFYVE19 deficiency—disordered cholangiocyte polarity and increased cell death—were revealed by the mouse model. Deficiency of ZFYVE19/Zfyve19 causes failure of cell division and increased cell death. This might cause release of a range of chemokines and macrophage activation via TGF-β signalling, leading to biliary fibrosis in ZFYVE19-deficient patients.

Acknowledgements We thank Dr A S Knisely for editing and proof-reading of the manuscript.

Contributors JY and YNZ: Conceptualisation, formal analysis, methodology, resources, visualisation and writing—original draft. RXW: Methodology and writing—reviewing and editing. CZH: Methodology and validation. YQ: Data curation, visualisation and resources. HC: Resources. WSL and XXS: Methodology. HYT and XJZ: Formal analysis. JAS and VL: Writing—reviewing and editing. MC: Conceptualisation, supervision, methodology and writing—reviewing and editing. JSW: Conceptualisation, supervision, writing—drafting and revision. All authors read and approved the final manuscript. JSW—the guarantor—has full access to the data, takes full responsibility for the integrity of the work and the conduct of the study, and controls the decision to publish.

Funding This research was partially or fully sponsored by the National Key Research and Development Program of China (Grant No. 2021YFC2700800), the National Natural Science Foundation of China (91954123 and 31972887), the Shanghai Municipal Science and Technology Major Project (19140901600) and Innovative research team of high-level local universities in Shanghai (SHSMU-ZDCX20211800).

Competing interests None declared.

Patient consent for publication Not applicable.

Ethics approval All animal-related protocols were approved by the committee of the care and use of laboratory animals in Children's Hospital of Fudan University (permit 2020-402), according to the guidelines of the Institutional Animal Care and Use Committee.

Provenance and peer review Not commissioned; externally peer reviewed.

Data availability statement All data relevant to the study are included in the article or uploaded as online supplemental information.

ORCID iDs
Jing Yang http://orcid.org/0000-0001-6739-951X
Yiling Qiu http://orcid.org/0000-0002-7296-9115
Wei-Sha Luan http://orcid.org/0000-0002-2130-6426
Victor Ling http://orcid.org/0000-0003-0823-586X
Muqing Cao http://orcid.org/0000-0002-0352-6548

REFERENCES

1 Luan W, Hao C-Z, Li J-Q, *et al*. Biallelic loss-of-function ZFYVE19 mutations are associated with congenital hepatic fibrosis, sclerosing cholangiopathy and high-GGT cholestasis. *J Med Genet* 2021;58:514–25.
2 Wen J. Congenital hepatic fibrosis in autosomal recessive polycystic kidney disease. *Clin Transl Sci* 2011;4:460–5.
3 Mandato C, Siano MA, Nazzaro L, *et al*. A ZFYVE19 gene mutation associated with neonatal cholestasis and cilia dysfunction: case report with a novel pathogenic variant. *Orphanet J Rare Dis* 2021;16:179.
4 Gan W, Liao B, Li X. A rare cause of liver fibrosis in adulthood. *Gastroenterology* 2022;162:e1–3.
5 Thoresen SB, Campsteijn C, Vietri M, *et al*. ANCHR mediates aurora-B-dependent abscission checkpoint control through retention of VPS4. *Nat Cell Biol* 2014;16:550–60.
6 Zong Y, Panikkar A, Xu J, *et al*. Notch signaling controls liver development by regulating biliary differentiation. *Development* 2009;136:1727–39.
7 Raynaud P, Tate J, Callens C, *et al*. A classification of ductal plate malformations based on distinct pathogenic mechanisms of biliary dysmorphogenesis. *Hepatology* 2011;53:1959–66.
8 Lemaigre FP. Development of the biliary tract. *Mech Dev* 2003;120:81–7.
9 Shin B, Kim MS, Lee Y, *et al*. Generation and fates of supernumerary centrioles in dividing cells. *Mol Cells* 2021;44:699–705.
10 Wiman KG, Zhivotovsky B. Understanding cell cycle and cell death regulation provides novel weapons against human diseases. *J Intern Med* 2017;281:483–95.
11 Baudoin NC, Nicholson JM, Soto K, *et al*. Asymmetric clustering of Centrosomes defines the early evolution of tetraploid cells. *Elife* 2020;9:e54565.
12 Tang L-Y, Heller M, Meng Z, *et al*. Transforming growth factor-beta (TGF-beta) directly activates the JAK1-STAT3 axis to induce hepatic fibrosis in coordination with the SMAD pathway. *J Biol Chem* 2017;292:4302–12.
13 Liu J, Wang F, Luo F. The role of JAK/STAT pathway in fibrotic diseases: molecular and cellular mechanisms. *Biomolecules* 2023;13:119.
14 Wang R, Lam P, Liu L, *et al*. Severe cholestasis induced by cholic acid feeding in knockout mice of sister of P-glycoprotein. *Hepatology* 2003;38:1489–99.
15 Joshi N, Ray JL, Kopec AK, *et al*. Dose-dependent effects of alpha-naphthylisothiocyanate disconnect biliary fibrosis from hepatocellular necrosis. *J Biochem Mol Toxicol* 2017;31:1–7.
16 Nigg EA, Holland AJ. Once and only once: mechanisms of centriole duplication and their deregulation in disease. *Nat Rev Mol Cell Biol* 2018;19:297–312.
17 Gunay-Aygun M. Liver and kidney disease in ciliopathies. *Am J Med Genet C Semin Med Genet* 2009;151C:296–306.
18 Galluzzi L, Vitale I, Aaronson SA, *et al*. Molecular mechanisms of cell death: recommendations of the nomenclature committee on cell death 2018. *Cell Death Differ* 2018;25:486–541.
19 Vitale I, Galluzzi L, Castedo M, *et al*. Mitotic catastrophe: a mechanism for avoiding genomic instability. *Nat Rev Mol Cell Biol* 2011;12:385–92.
20 Schwabe RF, Tabas I, Pajvani UB. Mechanisms of fibrosis development in nonalcoholic steatohepatitis. *Gastroenterology* 2020;158:1913–28.
21 Locatelli L, Cadamuro M, Spirlì C, *et al*. Macrophage recruitment by fibrocystin-defective biliary epithelial cells promotes portal fibrosis in congenital hepatic fibrosis. *Hepatology* 2016;63:965–82.
22 Fabregat I, Caballero-Díaz D. Transforming growth factor-beta-induced cell plasticity in liver fibrosis and hepatocarcinogenesis. *Front Oncol* 2018;8:357.
23 Caja L, Dituri F, Mancarella S, *et al*. TGF-beta and the tissue microenvironment: relevance in fibrosis and cancer. *Int J Mol Sci* 2018;19:1294.
24 Malyshev I, Malyshev Y. Current concept and update of the macrophage plasticity concept: intracellular mechanisms of reprogramming and M3 macrophage "switch" phenotype. *Biomed Res Int* 2015;2015:341308.